Available online at www.sciencedirect.com
SCIENCE DIRECT
Polymer 46 (2005) 6325–6334
polymer
www.elsevier.com/locate/polymer

Effects of clay orientation and aspect ratio on mechanical behavior of nylon-6 nanocomposite

J.-I. Weon, H.-J. Sue*

Department of Mechanical Engineering, Polymer Technology Center, Texas A & M University, College Station, TX 77843-3123, USA

Received 14 February 2005; received in revised form 21 May 2005; accepted 23 May 2005
Available online 14 June 2005

Abstract

The mechanical properties of nylon-6/clay nanocomposites with variations in clay aspect ratio and orientation were studied. A large-scale simple shear process was utilized to alter the clay aspect ratio and orientation within the reference nanocomposite. It was found that the modulus, strength, and heat distortion temperature of the nanocomposites decreased as the clay aspect ratio and degree of orientation were reduced. Furthermore, the reduction of clay aspect ratio and orientation led to an increase in fracture toughness and ductility. The Halpin–Tsai and Mori–Tanaka micromechanics-based models were implemented to gain a better understanding with regard to the dependence of clay structural parameters, i.e. aspect ratio and orientation, on the reinforcement effect of the nanofillers. The micromechanical models can accurately describe the relationship between clay structural parameters and the corresponding moduli for exfoliated nanocomposites.

Keywords: Nylon-6/clay nanocomposite; Aspect ratio; Orientation

1. Introduction

Filler-reinforced polymeric nanocomposite systems with well-dispersed inorganic nanoparticles typically exhibit significant improvements in physical and mechanical properties over their neat resin counterpart. The most commonly produced nanocomposite systems are polymer-layered silicate nanocomposites, which are of interest because of their exceptional reinforcement effects at very low clay loading. This characteristic has been exploited to prepare commercially viable structural components since minimized nanofiller loading results in a lighter structure, good processability, and increased ductility. Moreover, a negligible loss in fracture toughness is usually observed in such nanocomposite systems [1].

Layered silicates are composed of extremely thin ($\sim$1 nm), plate-like structures that have large surface areas and high aspect ratios. In addition, the platelets have an exceptionally high modulus compared to that of the surrounding polymer matrix. The reinforcement effect of polymer nanocomposites strongly depends on the filler's structural parameters, such as shape, aspect ratio, modulus, volume fraction, interfacial adhesion, surface characteristics and orientation [2–6]. Recent research efforts have focused on developing well-exfoliated nanocomposites using various processing techniques (e.g. in situ polymerization [7–9], emulsion polymerization [10,11], melt compounding [12–14], and sol-gel processing methods [15–17]); only limited success has been achieved [18–27]. Fornes et al. [26] investigated the effect of organic surfactant structure and molecular weights of nylon-6 on the mechanical properties of nylon-6 nanocomposites. Sue et al. [27] reported that, for α-zirconium phosphate-based epoxy nanocomposites, surface modifiers had a significant effect on the thermal properties and toughening mechanisms of the nanocomposites.

Using micromechanics-based composite models, a few of recent studies [28,29] have attempted to examine how the nanofiller structural parameters (e.g. shape, aspect ratio and orientation) affect the mechanical properties. Although these micro-mechanical models cannot be used to fully account for the exact mechanical behavior of polymer nanocomposites, it generally gives satisfactory correlations. Yet, there is no experimental effort within the literature to address how the aspect ratio and orientation of clay layered

* Corresponding author. Tel.: +1 979 845 5024; fax: +1 979 862 3989.
E-mail address: hjsue@tamu.edu (H.-J. Sue).

0032-3861/$ - see front matter © 2005 Elsevier Ltd. All rights reserved.
doi:10.1016/j.polymer.2005.05.094

structures affect mechanical properties of polymer nanocomposites. This is partially owed to the fact that it is nontrivial to experimentally control the aspect ratio and orientation of nanoscopic fillers in a polymer matrix without simultaneously changing other material parameters. Therefore, there is a significant interest to experimentally prepare variations in nanofiller aspect ratios and orientations in polymer nanocomposites and study how they influence mechanical properties.

It has been shown that the presence of clay layers may affect the nucleation and growth of crystalline lamellae in nylon, resulting in the formation of complex morphologies within the matrix. Kojima et al. [1] found that the γ-crystalline phase would dominate when clay layers are dispersed in a nylon matrix, whereas neat nylon-6 exhibits a high level of α-form crystalline structure. Because it has been well-established that lamellar orientation can greatly affect the mechanical properties of semi-crystalline polymers, it is important to determine the nanoscale morphological characteristics of crystalline lamellar orientation as well as the clay orientation in nylon-6/clay nanocomposite.

The present paper attempts to study how the aspect ratio and orientation of clay layered structures affect the mechanical properties of nylon-6/clay nanocomposites. Characterization of nylon-6/clay nanocomposite morphology is presented elsewhere [30]. Creasy et al. [31] found that a large-scale simple shear process can control the fiber orientation of glass fiber/polyacetal composites, depending on the processing routes. Xia [32] also speculated that controlled nanoparticle orientation could be easily achieved through a simple shear process. The same simple shear process was, therefore, carried out to alter clay aspect ratios and orientations within the nylon-6 matrix.

Both the Halpin–Tsai and Mori–Tanaka micromechanics-based composite models were implemented to account for the effect of the nanofiller structural parameters on the reinforcement of the nanocomposites. The fundamental structure-property relationship of polymer nanocomposites, based on this micromechanical model, is discussed.

2. Continuum-based micromechanical models

A number of micro-mechanical composite models have been developed to describe the macroscopic mechanical properties of discontinuous, filler-based composites [33–43]. Many assumptions are inherent in these micromechanical models. The detailed description and discussion of assumptions of these micromechanical models have been documented [29]. In conventional micromechanical models, filler volume fraction (ϕ_f), aspect ratio (α), orientation (S), and modulus (E_f) are important factors for describing the macroscopic composite properties. Tucker et al. [44] reviewed the application of several composite models for fiber-reinforced composites. They reported that the Halpin–Tsai theory [39–41] offered reasonable predictions for composite modulus. The model proposed by Mori–Tanaka [36,38] exhibited better predictive capabilities for fillers with relatively high aspect ratios. The longitudinal engineering modulus (E_{11}) of the Halpin–Tsai and the Mori–Tanaka model are expressed in Eqs. (1) and (2), respectively

$$\frac{E_{11}}{E_m} = \frac{1 + 2(l/t_p)\eta\phi_f}{1 - \eta\phi_f} \tag{1}$$

$$\eta = \frac{E_f/E_m - 1}{E_f/E_m + 2(l/t_p)}$$

where l is filler length and t_p is filler thickness; and

$$\frac{E_{11}}{E_m} = \frac{1}{1 + \phi_f[-2\nu_m A_3 + (1 - \nu_m)A_4 + (1 + \nu_m)A_5 A]/2A} \tag{2}$$

where ϕ_f is filler volume fraction, ν_m is the Poisson's ratio of the matrix, and A, A_3, A_4, and A_5 are calculated from the matrix and filler properties and the components of the Eshelby tensor [34]. The above models were utilized to describe the clay reinforcement effect in nylon-6/clay nanocomposites.

3. Experimental

3.1. Materials

Commercially available nylon-6/clay nanocomposite pellets containing 2 wt% of layered silicate clay (commercial grade, 1022C2) and neat nylon-6 (commercial grade, 1022B) were provided by Ube Industries, Japan. The detailed description and the overall process for preparing the resin and nanocomposite are documented in Refs. [7,45]. Briefly, organic, surface-modified montmorillonite clay was prepared via a cation-exchange reaction with 12-aminolauric acid. The resulting ion-exchanged montmorillonite clay (termed 12-montmorillonite) was mixed with ε-caprolactam. Ring-opening polymerization of the ε-caprolactam, with addition of a small amount of 6-aminocaproic acid, was initiated by carboxyl ends (–COOH) of the 12-montmorillonite clay, resulting in the chains (~32% of nylon-6 chains) with cationic ammonium ends ($-NH_3^+$) tethered to the surface of negatively charged layer silicates.

3.2. Sample preparation

Pellets of the neat nylon-6 and nylon-6/clay nanocomposite were dried at 100 °C for 12 h, and were then slowly injection molded using a custom-built extrusion-injection molding machine powered by a HaakeBuchler Rheocord (system 40) machine with a screw revolving at 30 rpm. The temperature profiles of the extruder barrel were set at

235–245–255–260 °C progressively toward the inlet of the injection mold, with the mold temperature set at 180 °C. After molding, the samples were immediately sealed in a polyethylene bag and kept in a vacuum desiccator prior to use to avoid moisture absorption.

A large-scale simple shear process, termed equal channel angular extrusion (ECAE) [31,32], was performed to alter the aspect ratio and orientation of the clay nanoparticles. This ECAE process was carried out at 60 °C and at an extrusion rate of 0.25 mm/s using a servo-hydraulic mechanical system (MTS-810). The samples before and after ECAE were categorized as follow: (1) reference, (2) A1-received a single ECAE pass, and (3) C2-received two ECAE passes with a 180° rotation of specimen between the passes (Fig. 1). Detailed description of the ECAE simple shear process can be found in Refs. [32,46–51]. After the sample preparation, all samples were annealed at 150 °C for 3 h to minimize any pre-existing molecular and clay orientation in the matrix due to processing [52–56]. Furthermore, the annealing chamber was purged with nitrogen gas to minimize sample oxidation during annealing. After annealing, the specimens were cut to an appropriate size and polished to desired dimensions for mechanical testing and structural characterizations.

3.3. Microscopy and image analysis

Transmission electron microscopy (TEM) observations were conducted on a JEOL JEM-2010A TEM operating at an accelerating voltage of 200 kV. Ultra-thin sections of ~90 nm in thickness of nylon-6 nanocomposite were obtained, under cryogenic condition, using a Reichert–Jung Ultracut E microtome. A diamond knife was used for the thin-sectioning, and the thin-sections were placed on 100-mesh Formvar/carbon-coated copper grids for TEM observation. Note that samples for TEM analysis were cut parallel to the ND–FD plane, as depicted in Fig. 2.

In order to determine the clay aspect ratio and degree of clay orientation in nylon-6/clay nanocomposites, a semi-automated image analysis procedure, described by Fornes et al. [26,29], was carried out.

3.4. Mechanical testing

Tensile properties were evaluated at room temperature according to ASTM-D638-02. The tensile specimens cut parallel to the flow direction (Fig. 2) were tested using a screw-driven mechanical testing machine (Sintech II) at a constant crosshead speed of 0.085 mm/s (0.2 in./min). An extensometer was used to measure the displacement in the gauge region. Young's modulus was calculated at 1% strain, and yield stress and elongation at break were determined in accordance with the above ASTM standard. The average values and standard deviations were determined from testing five specimens of each sample.

The stress intensity factor (K_{IC}) of the samples was obtained according to ASTM-D5045-99, with the K_{IC} specimens in a single-edge-notch 3-point-bend (SEN-3PB) geometry. By tapping a liquid-nitrogen-chilled razor blade into the wedge, thumb nail-shaped sharp cracks were

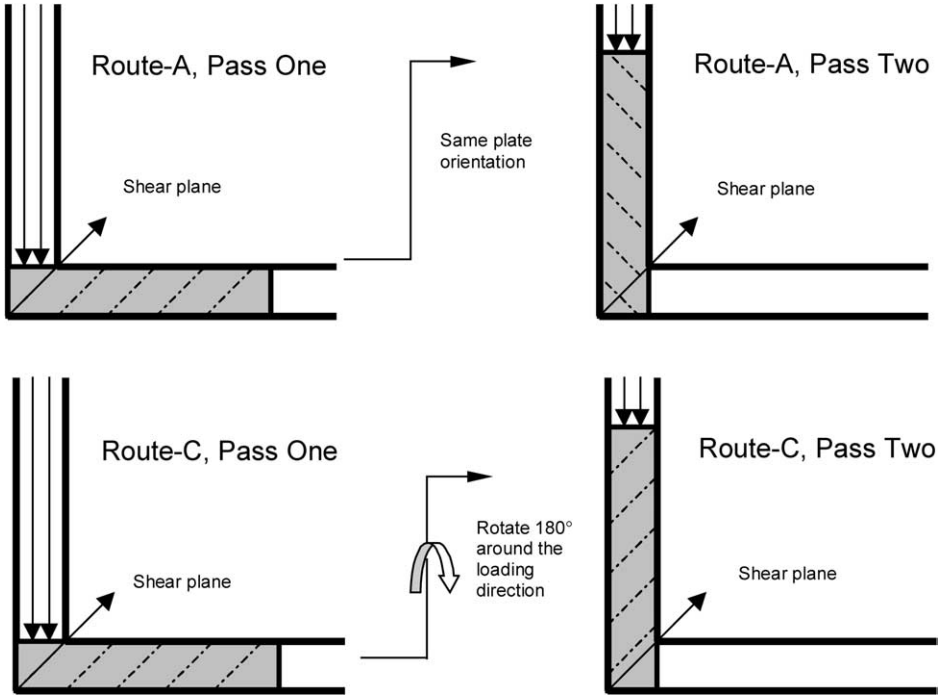

Fig. 1. Schematic of route A- and route C-ECAE processes.

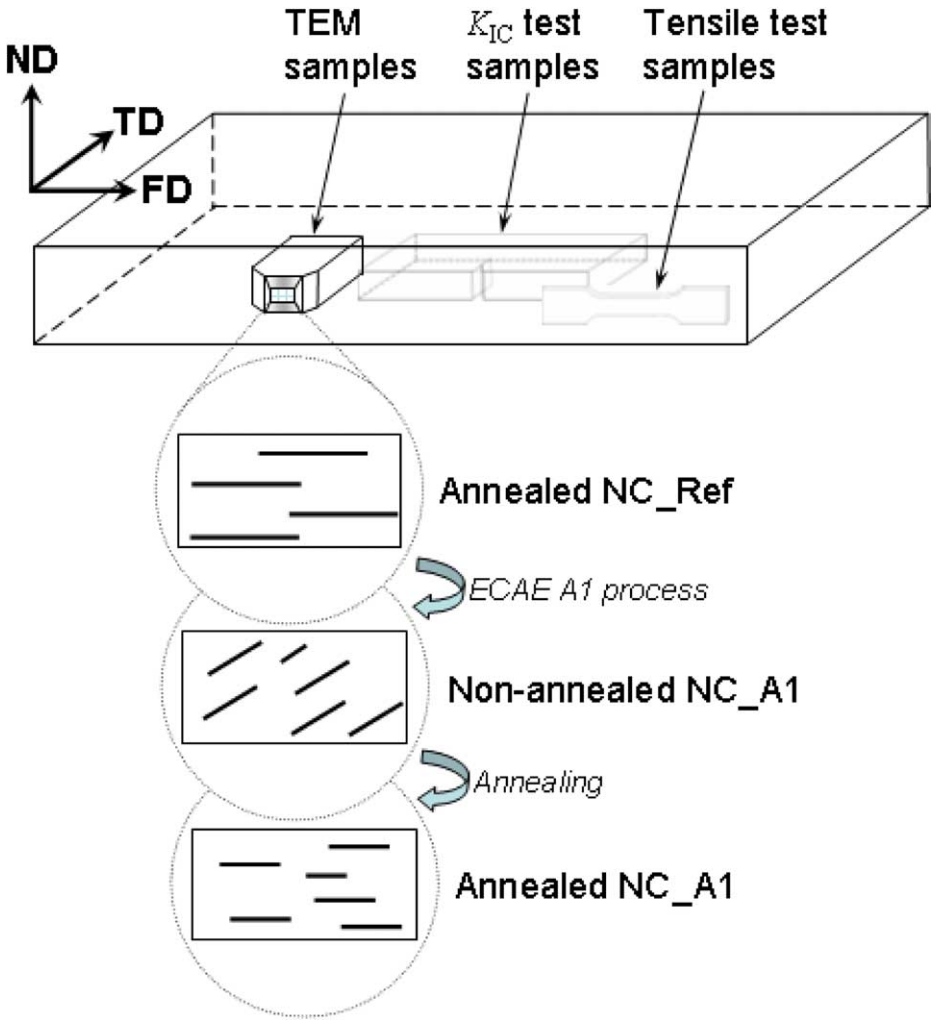

Fig. 2. Schematic of the specimens used for tensile, K_{IC} testing, and TEM observation, and the clay orientation with respect to the ECAE processing and annealing; ND, normal direction; TD, transverse direction and FD, flow direction.

generated. The ratio of the initial crack length (a) to the specimen width (W), a/W, was fixed between 0.4 and 0.6. The crack propagation was parallel to the transverse direction (Fig. 2). Five specimens from each sample were tested at room temperature and at a crosshead speed of 10 mm/min, using a screw-driven mechanical testing machine (Instron Model 1125).

The dynamic mechanical analysis (DMA) tests were performed under torsional mode on a rheometric mechanical spectrometer (RMS-800) at temperatures ranging from −140 to 250 °C. The DMA specimens were cut parallel to the flow direction. Measurements were made at 5 °C per step with 45 s of soaking time. The spectrometer was set to produce a sinusoidal wave function with a peak strain of 0.1% and frequency of 1 Hz. The storage moduli versus temperature and tan δ versus temperature profiles were recorded and reported. The glass transition temperature, T_g, was determined based on the maximum tan δ peak temperature of the tan δ versus temperature curve.

4. Results and discussion

4.1. Microscopy investigation and image analysis

The morphology characterization of nylon-6/clay nanocomposite before and after ECAE process, and before and after annealing, has been described elsewhere [30]. Only the final morphologies of the nanocomposites are briefly reported here.

Fig. 2 shows the schematic of clay orientation with respect to the ECAE processing direction. It should be noted that after a one-pass (A1) ECAE process which induced the maximum shear strain of 180%, the shortened clay layers are aligned nearly parallel to the maximum simple shear plane [50], i.e. at an angle (θ) of $\sim$26° counter-clockwise away from the flow direction (FD). However, after annealing, the clay orientation becomes parallel to the FD. This clay orientation recovery is most likely due to the thermally activated relaxation of molecular/lamellar

orientation of the nylon-6 matrix and the pre-existing residual stresses [50,51]. Figs. 3 and 4 show the TEM micrographs that indicate different clay aspect ratios and orientations of the ECAE-processed nanocomposite samples before and after annealing. The reference nylon-6/clay nanocomposite, which received no ECAE simple shear deformation, exhibits a well-exfoliated clay structure with an orientation along the FD (Figs. 3(a) and 4(a)). Also, it is observed that the clay lengths and orientations of the A1 and C2 nylon-6/clay nanocomposites have been altered upon the ECAE simple shear process.

Fig. 5 shows the schematic of lamellar orientation with respect to the ECAE processing direction. The exfoliated nanocomposites exhibit a global orientation of clay layers,

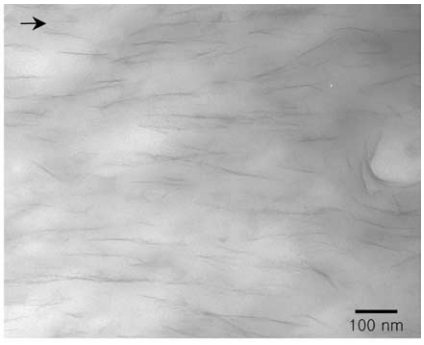

(a)

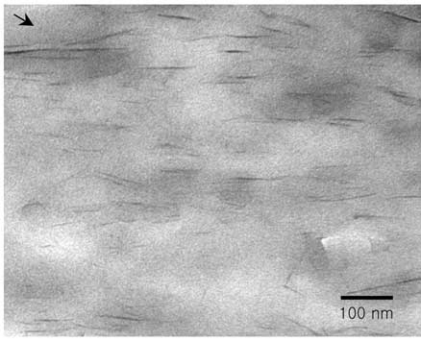

(b)

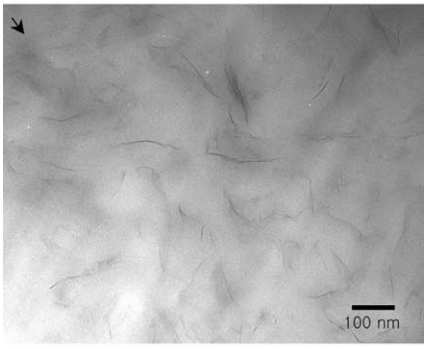

(c)

Fig. 3. Typical TEM micrographs of the simple-shear-processed and non-annealed nylon-6/clay nanocomposites (NC) used for image analysis: (a) NC_Reference, (b) NC_A1 and (c) NC_C2. The arrows indicate the flow direction.

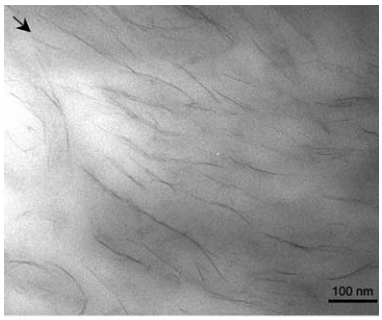

(a)

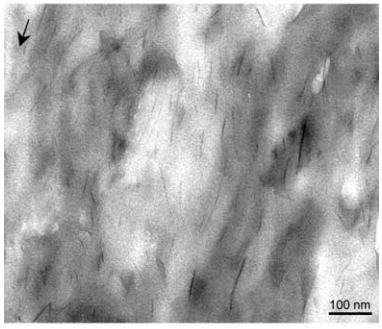

(b)

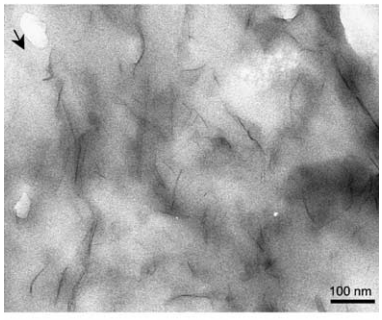

(c)

Fig. 4. Typical TEM micrographs of the simple-shear-processed and annealed nylon-6/clay nanocomposites (NC) used for image analysis: (a) NC_Reference, (b) NC_A1 and (c) NC_C2. The arrows indicate the flow direction.

arising from the flow-induced alignment and local orientation of crystalline lamellae caused by the clay particles. The annealed reference nanocomposite shows that the crystalline lamellae are oriented preferentially along $\sim 41^{\circ}$ counter-clockwise away from the clay orientation. For the annealed A1 and C2 nanocomposites, a reduction in clay aspect ratio helps to form another weak preferred lamellar orientation, which is almost perpendicular to the clay layer orientation. In addition, a misalignment in clay orientation leads to a more randomized lamellar orientation in the annealed C2 nanocomposite. The detailed experimental procedure for obtaining the above morphological features is reported elsewhere [30].

It is interesting to note that the C2-ECAE simple shear process can exert highly localized stresses to reduce the aspect ratio of clay. Fig. 6 shows the fractured clay layers

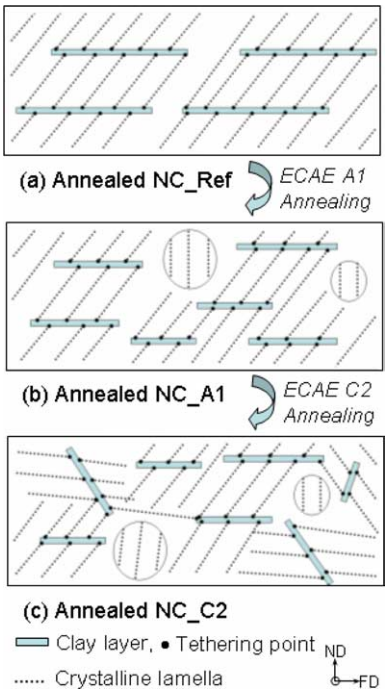

Fig. 5. Schematic of the lamellar orientation with respect to the ECAE processes and annealing.

after the C2-ECAE process, thus greatly reducing the aspect ratio of clay in the matrix.

A semi-automated image analysis scheme was performed to quantify these morphological variations. It should be mentioned that three different TEM micrographs from three different locations of each sample were used to ensure the reliability of the image analysis. The distribution and statistical box plot of the platelet length for the annealed samples of the reference, A1, and C2 nanocomposites are shown in Fig. 7(a). The aspect ratios (α) of dispersed platelets are determined by:

$$\alpha = \bar{l}/\bar{h} \tag{3}$$

where $\bar{l}$ is mean platelet length and $\bar{t}$ is mean platelet thickness.

It is well known that the commercial Ube nylon-6/clay nanocomposite used in this study is a fully exfoliated system. Thus, it is safe to take the mean platelet thickness to be 0.94 nm, which is the single layer thickness of the clay [29].

Fig. 7(b) shows the distribution and statistical boxplot of the degree of platelet orientation in the reference, A1, and C2 annealed nanocomposites. The degree of platelet orientation (S) is defined as

$$S = \sqrt{\frac{\sum_{i=1}^{n}(\Phi_i - \bar{\Phi})^2}{N}} \tag{4}$$

(i.e. standard deviation), where Φ_i is the actual platelet orientation ($0° \le \Phi \le 90°$), $\bar{\Phi}$ is the mean platelet orientation,

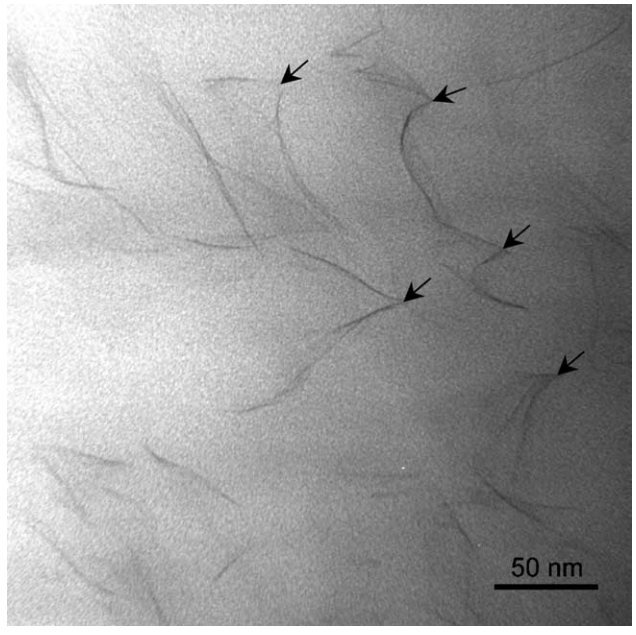

Fig. 6. TEM micrograph showing the fractured and shortened clays via an ECAE simple shear process. The arrows indicate the fractured clays.

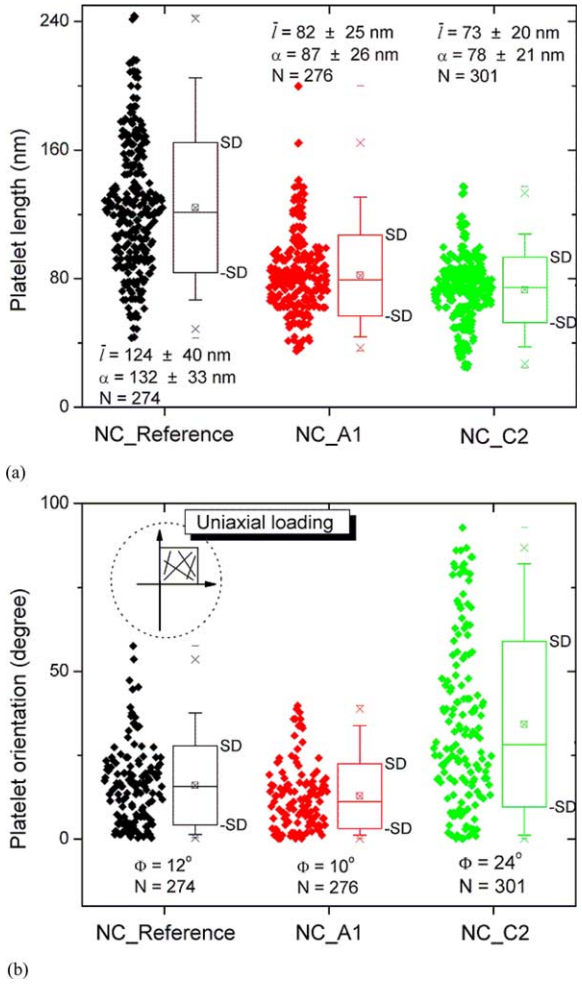

Fig. 7. Quantitative TEM image analyses of the annealed nanocomposites: (a) clay length and (b) clay orientation (SD: standard deviation).

and N is total number of platelets counted. It should be noticed that the degree of platelet orientation was determined in relation to the uniaxial tension orientation on which the tensile tests were performed.

The results of the image analyses are summarized in Table 1. Interestingly, these results indicate that the A1 process only reduces the clay aspect ratio, while the C2 route alters not only the clay aspect ratio but also the clay orientation due to the accumulated crisscross residual plastic deformation generated by an additional ECAE process with 180° rotation of the specimen (Fig. 1). It is noted that although there is little difference in clay aspect ratio, there is a slight variation in degree of orientation between the reference and annealed nanocomposites. This discrepancy may be caused by the relaxation of nylon-6 matrix during sample annealing. The details of the morphological characterization can be found elsewhere [30].

4.2. Mechanical properties

Typical engineering stress–strain curves and their key tensile property dependence on clay aspect ratio and orientation are shown in Fig. 8 and Table 2. All of the specimens tested were annealed samples. A decrease in aspect ratio from 132 to 87 causes an obvious reduction in modulus and yield stress. However, a slight increase in elongation at break is also observed. In addition to the change in aspect ratio, the degree of clay orientation has an effect on tensile properties. The annealed C2 nanocomposite, which has a more randomly dispersed clay and lower aspect ratio, exhibits a much lower modulus (~19%) and yield stress (~10%) than those of the annealed reference nanocomposite. For comparison purposes, the Young's modulus and the yield stress of non-annealed A1 nylon-6 are given to be 3.03±0.13 GPa and 77.2±1.7 MPa, respectively. These values are not much different from the annealed nylon-6 since the ECAE process on semi-crystalline polymers tends to only destroy spherulites and cause some lamellar orientation. No significant molecular orientation throughout the sample is observed [32,49–51]. Fig. 9 highlights the influences of clay aspect ratio and degree of clay orientation on the tensile properties. When normalized by the tensile modulus of the reference nanocomposite, a decrease in aspect ratio results in a distinctive decrease in Young's modulus. On the other hand, a large decrease (100%) in alignment of clay, seen in the C2 nanocomposite, seems to have a relatively small effect (≈8%) on tensile modulus. Based on the above finding, the effect of clay aspect ratio on tensile properties appears to be more significant.

Table 1
The results of TEM image analysis for the reference, A1, and C2 nanocomposites

Sample	Aspect ratio (α)		Degree of orientation[a] (S)	
	Annealing			
	Before	After	Before (°)	After (°)
NC_Ref	131±37	132±33	8	12
NC_A1	89±24	87±26	7	10
NC_C2	80±25	78±21	25	24

[a] Degree of platelet orientation from unidirectional reinforcement.

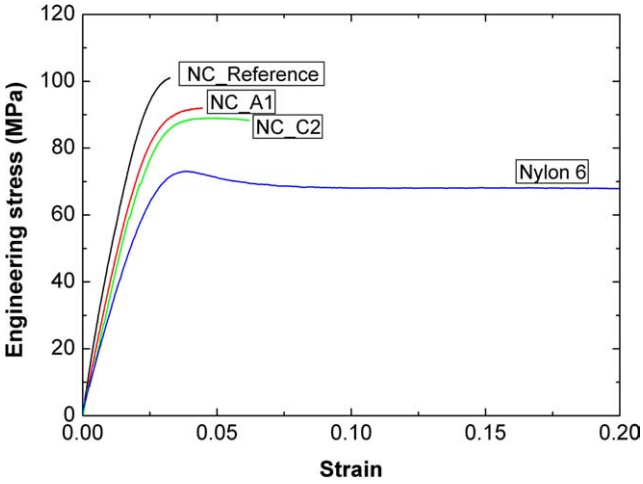

Fig. 8. Typical engineering stress–strain curves for the annealed neat nylon-6 and nanocomposites.

The K_{IC} values for the annealed nanocomposites are given in Table 3. A reduction in aspect ratio and alignment of clay results in an improved fracture toughness. It is interesting to note that the clay orientation perpendicular to the crack propagation direction does not seem to improve fracture toughness. This suggests that the natural crack tip radius of the nylon-6/clay nanocomposite is too large compared to the clay dimensions to show an effect.

The dynamic mechanical properties for the annealed neat nylon-6 and nanocomposites are shown in Fig. 10. There is virtually no difference in T_g variation among the nanocomposites investigated. The addition of clay results in a significant increase in storage moduli throughout the whole temperature range studied (Table 3). The reinforcing effect of clay aspect ratio and orientation appears to be the highest at temperatures above T_g. This may be due to the fact that the exfoliated clay is most effective in resisting the mobility of the nylon-6 molecules above T_g.

The heat distortion temperature (HDT), defined as a deflection-temperature at which polymeric materials

Table 2
Tensile properties of the neat nylon-6 and nylon-6/clay nanocomposites

Sample	Young's modulus[a] (GPa)	Yield stress[a] (MPa)	Elongation at break (%)
NC_Ref	4.67±0.20	98.2±2.3	4.7
NC_A1	4.09±0.18	93.0±1.3	5.3
NC_C2	3.80±0.14	88.9±2.4	5.8
Nylon-6	3.14±0.11	76.4±1.2	45

[a] Standard deviation for the five samples tested.

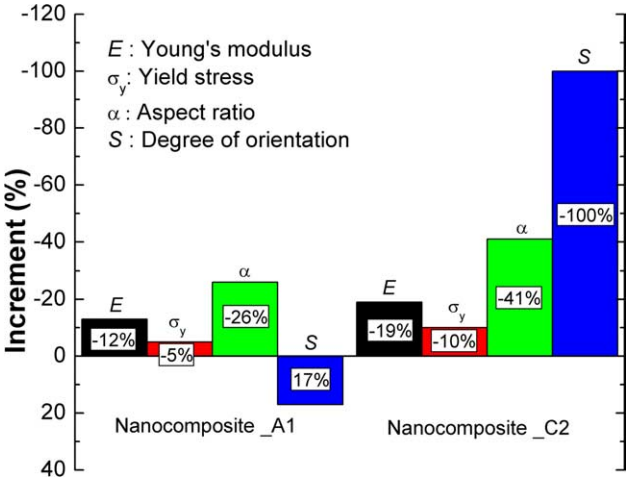

Fig. 9. Effect of clay aspect ratio and clay orientation on tensile properties for the ECAE-processed and annealed nanocomposites.

undergo an arbitrary deformation under a constant load, is one of the key indicators that can address load-bearing capabilities at elevated temperatures. Fig. 10(b) illustrates HDT values obtained from the storage modulus versus temperature curve of DMA results [57]. A significant increase in HDT is observed in the annealed reference nanocomposite (Table 3), implying that high aspect ratios of nanofillers yields a significant increases in HTD.

It is noted that the lamellar orientations and crystallinity of nylon-6 [30] in the nanocomposites investigated remain more or less the same after annealing. Consequently, the ECAE process is unlikely to cause any significant changes in matrix properties. The mechanical properties variations reported above should, therefore, be mainly due to the changes in clay aspect ratios and orientations.

4.3. Effective filler-based micromechanical models

The dispersion of fillers in a matrix is typically described in terms of exfoliation or intercalation. The fully exfoliated nanocomposites are considered to consist of single clay layers dispersed in a polymer matrix. While in the intercalated systems, inter-layer domains of fillers are typically penetrated by polymer chains and consequently stacked with an inter-layer spacing of 1–4 nm. However,

Table 3
Mechanical properties and heat distortion temperature of the neat nylon-6 and nylon-6/clay nanocomposites

Sample	Storage modulus, G' (Pa)		K_{IC}[a] (MPa m$^{0.5}$)	HDT (°C)
	25 °C	100 °C		
NC_Ref	1.28×10^9	3.33×10^8	2.7 ± 0.07	110
NC_A1	1.12×10^9	2.89×10^8	3.1 ± 0.13	90
NC_C2	1.07×10^9	2.51×10^8	3.0 ± 0.11	84
Nylon-6	1.05×10^9	1.94×10^8	3.0[b]	75

[a] Standard deviation for the five samples tested.
[b] The value is quoted from Ref. [61].

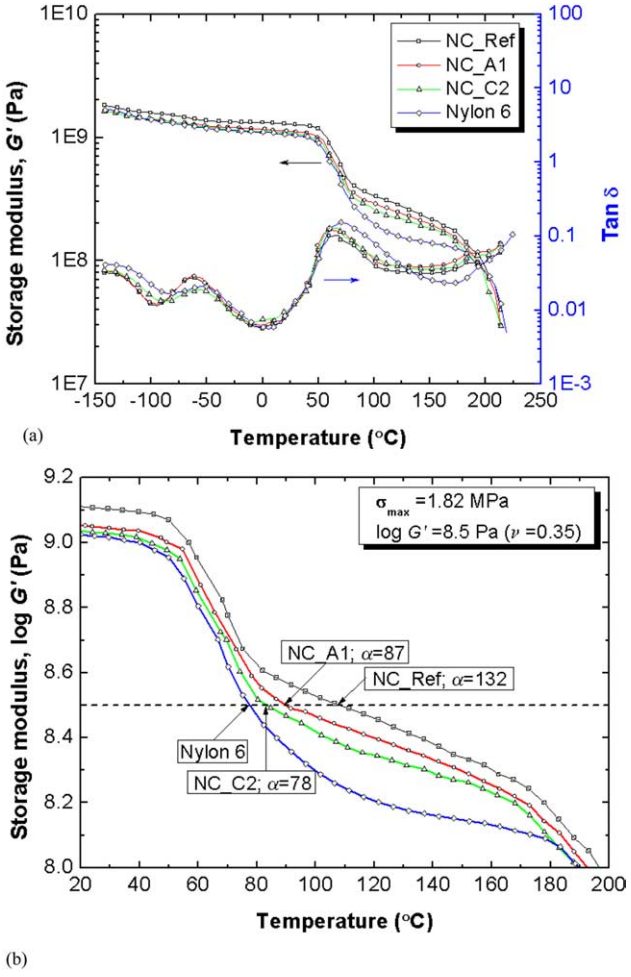

Fig. 10. Dynamic mechanical spectra for the annealed neat nylon-6 and nanocomposites: (a) storage modulus and loss tangent and (b) the HDT estimated from the plot of log G' versus temperature.

conventional filler-based micromechanical models for predicting the modulus of nanocomposites do not consider the clay structural characteristics. Here, typical effective filler structural parameters are defined by the number of platelets per stacked clay (n) and the platelets inter-layer spacing (d_{001}); these parameters can be used to account for mechanical property enhancement for both exfoliated and intercalated nanocomposites. The mechanics-based model for effective filler structure is established by mapping the effective filler structural parameters (n, d_{001}) to the conventional filler structural parameters (α, ϕ_f, E_f).

The thickness of effective filler can be expressed in terms of n and d_{001} by the following equation [29]:

$$t_{\text{eff}} = (n-1)d_{001} + t_p \tag{5}$$

The effective filler aspect ratio (α_{eff}), volume fraction (ϕ_{eff}) and modulus (E_f^{eff}) can be written as [28]:

$$\alpha_{\text{eff}} = \frac{l}{t_{\text{eff}}} = \frac{l}{(n-1)d_{001} + t_p} \tag{6}$$

$$\phi_{\text{eff}} = \frac{\psi_{\text{eff}}[(n-1)d_{001} + t_{\text{p}}]}{nt_{\text{p}}} \frac{\rho_{\text{m}}}{\rho_{\text{f}}} \tag{7}$$

$$E_{\text{f}}^{\text{eff}} = \frac{nt_{\text{p}}E_{\text{f}}}{[(n-1)d_{001} + t_{\text{p}}]} \tag{8}$$

where ψ_{eff} is effective filler weight fraction and ρ_{f} and ρ_{m} are the densities of the filler and matrix, respectively. The influence of filler effective aspect ratio (α_{eff}) and orientation (S) on the modulus improvement was examined using the Halpin–Tsai (H–T) and Mori–Tanaka (M–T) theories. Similar trends are observed in the parametric study plots for both models (Fig. 11). The improved reinforcement efficiency is observed with the higher aspect ratio fillers. However, the Mori–Tanaka model is more conservative in estimation than the Halpin–Tsai model. This difference may originate from the discrepancies between assumptions inherent in the two models [29]. To compensate for these disparities, an adjustment of shape parameter ($2l/t_{\text{p}}$) in the Halpin–Tsai equation may be used. It should be noticed that E_{11}/E_{m} increases non-linearly with α_{eff} for both models (Fig. 11(a)). This underlying phenomenon may be explained by the load-transfer mechanism. The nature of these physics was well addressed in Ref. [28] using the shear lag model [42]. It should be mentioned that when the aspect ratios are 87 and 132, the clay length is sufficient for maximum load-transfer.

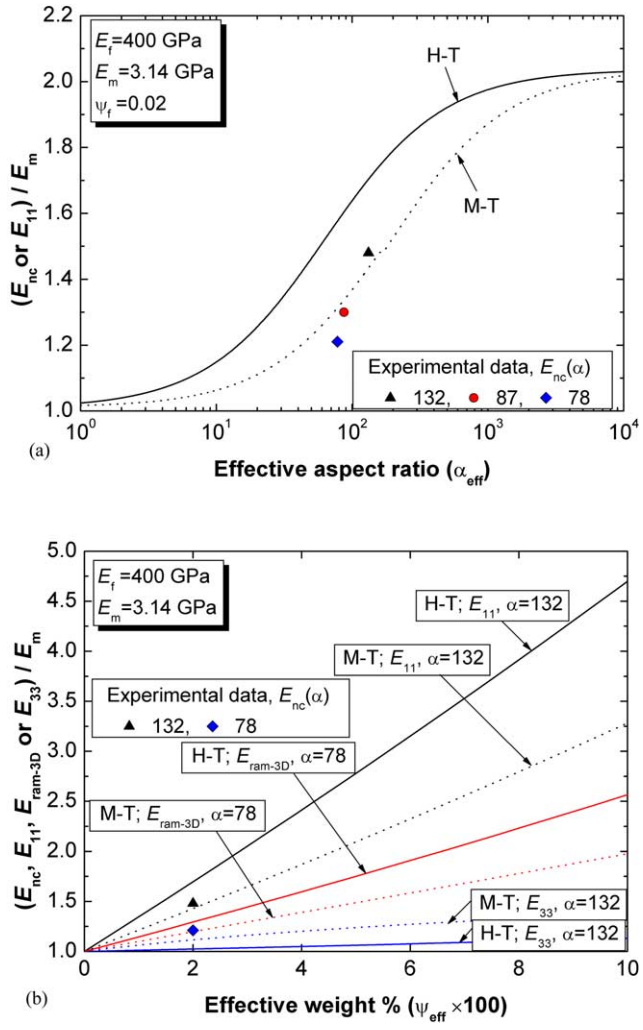

Fig. 11. Effective filler-based model predictions of the Halpin–Tsai (H–T) and the Mori–Tanaka (M–T) theories: (a) clay aspect ratio (α), and (b) clay orientation (S) on the modulus improvement of exfoliated nanocomposites. Experimental data (E_{nc}) included.

Disk-shaped platelets provide the same reinforcement in the two orthogonal directions; E_{11} and E_{22}. In the case of randomly oriented platelets, the following equation was proposed [58,59]:

$$E_{\text{radom-3D}}^{\text{platelet}} = 0.49E_{11} + 0.51E_{33} \tag{9}$$

The effect of filler orientation (S) on modulus enhancement of nanocomposite was examined using the Halpin–Tsai and Mori–Tanaka theories (Fig. 11(b)). It was found that misalignment of unidirectional reinforcement leads to detectable modulus reductions. Experimental results are compared with model predictions from the Halpin–Tsai and Mori–Tanaka theories (Fig. 11). In the case of the clay filler modulus, E_{f}, it has been estimated to be 400 GPa based on molecular dynamic simulation [60]. The predictions of Mori–Tanaka model are in good agreement with the experimental data. Conversely, the Halpin–Tsai model slightly over predicts the results. Note that the data for an aspect ratio of 78 in Fig. 11(a) needs to shift slightly to the left since the clay in the nanocomposite is more randomly oriented. It is also observed that the modulus of the C2 nanocomposite is in good agreement with the case for the radom-3D orientation.

Both experimental observations and micro-mechanical model predictions carried out in this study have clearly indicated that clay aspect ratio and orientation significantly affect the nanocomposite modulus. A high aspect ratio and unidirectional orientation lead to significantly improved moduli. Consequently, it is desirable to prepare polymer nanocomposites that exhibit full exfoliation with a preferred orientation along the tensile direction for maximum reinforcement effect.

5. Conclusions

Effects of aspect ratio and orientation on mechanical properties of nylon-6/clay nanocomposites were investigated. The aspect ratio and orientation of clay layers in naylon-6 matrix appear to be responsible for variations in mechanical properties. Unidirectional reinforcement and higher aspect ratios can lead to significant improvements in modulus, strength and heat distortion temperature, with a marginal loss in ductility. The effective filler-based Mori–Tanaka model offers a reasonably accurate prediction to account for modulus enhancement of the nanocomposites, which is consistent with experimental findings. Further, the

model may be used to predict elastic properties of other types of polymer nanocomposites. The ECAE simple process appears to be an effective method for tailoring clay aspect ratios and orientations in nylon-6. The clay aspect ratio and orientation are dominating factors responsible for mechanical property improvements of these polymer nanocomposites.

Acknowledgements

The authors would like to thank Ube Industries for providing the pellets of nylon-6/clay nanocomposite. Special thanks are also given to the Defense Logistic Agency (SP0103-02-D-0024) and the State of Texas ARP Grant (000512-00137-2001) for their financial support.

References

[1] Kojima Y, Usuki A, Kawasumi M, Okada A, Fukushima Y, Kurauchi T, et al. J Mater Res 1993;8:1185.
[2] Silva A, Rocha M, Moraes M, Valente C, Coutinho F. Polym Test 2000;21:57.
[3] Kim GM, Lee DH, Hoffmann B, Kressler J, Stöppelmann G. Polymer 2000;42:1095.
[4] Wang Y, Zhang L, Tang C, Yu D. J Appl Polym Sci 2000;78:1878.
[5] Fu X, Qutubuddin S. Polymer 2001;42:807.
[6] Mencel J, Varga J. J Therm Anal 1983;28:161.
[7] Usuki A, Kojima Y, Kawasumi M, Okada A, Fukushima Y, Kurauchi T, et al. J Mater Res 1993;8(5):1179.
[8] Kojima Y, Usuki A, Kawasumi M, Okada A, Kurauchi T, Kamigaito O. J Appl Polym Sci 1993;49:1259.
[9] Weimer MW, Chen H, Giannelis EP, Sogah DY. J Am Chem Soc 1999;121:1615.
[10] Lee DC, Jang LW. J Appl Polym Sci 1996;61:1117.
[11] Lee DC, Jang LW. J Appl Polym Sci 1998;68:1997.
[12] Liu L, Qi Z, Zhu X. J Appl Polym Sci 1999;71:1133.
[13] Vaia RA, Ishii H, Giannelis EP. Chem Mater 1993;5:1694.
[14] Christiani BR, Maxfield M. US Patent 5747560; 1998.
[15] Gregar KC, Winans RE, Botto RE. US Patent 5308808; 1994.
[16] Carrado KA, Xu L. Chem Mater 1998;10:1440.
[17] Okada A, Fukushima Y, Kawasumi M, Inagaki S, Usuki A, Sugiyami S, et al. US Patent 4739007; 1988.
[18] Sue HJ, Gam KT, Bestaoui N, Spurr N, Clearfield A. Chem Mater 2004;16(2):242.
[19] Weimer MW, Chen H, Giannelis EP, Sogah DY. J Am Chem Soc 1999;121(7):1615.
[20] Yano K, Usuki A, Okada A, Kurauchi T, Kamigaito O. J Polym Sci Part A: Polym Chem 1993;31(10):2493.
[21] Yano K, Usuki A, Okada A. J Polym Sci Part A: Polym Chem 1997; 35(11):2289.
[22] Delozier DM, Orwoll RA, Cahoon JF, Johnston NJ, Smith JG, Connell JW. Polymer 2001;43(3):813.
[23] Messersmith PB, Giannelis EP. Chem Mater 1994;6(10):1719.
[24] Lan T, Pinnavaia TJ. Chem Mater 1994;6(12):2216.
[25] Wang Z, Pinnavaia TJ. Chem Mater 1998;10(7):1820.
[26] Fornes TD, Yoon PJ, Keskkula H, Paul DR. Polymer 2001;42:9929.
[27] Sue HJ, Gam KT, Bestaoui N, Clearfield A, Miyamoto M, Miyatake N. Acta Mater 2004;52:2239.
[28] Sheng N, Boyce MC, Parks DM, Rutledge GC, Abes JI, Cohen RE. Polymer 2003;44:4993.
[29] Fornes TD, Paul DR. Polymer 2003;44:4993.
[30] Weon JI, Xia ZY, Sue HJ. J Polym Sci Part B: Polym Phys, submitted for publication.
[31] Creasy TS, Kang YS. J Thermoplast Compos Mater 2004;17:205.
[32] Xia ZY. Processing–structure–property relationships in oriented polymers, PhD Dissertation, Texas A and M University, Department of Mechanical Engineering; 2001.
[33] Adams D, Doner D. J Compos Mater 1967;1(4):152.
[34] Eshelby JD. Proc R Soc A 1957;241:376.
[35] Hill R. J Mech Phys Solids 1965;13:213.
[36] Tandon GP, Weng GJ. Polym Compos 1984;5(4):327.
[37] Hermans J. J Proc Kon Ned Akad v Wetensch B 1967;65:1.
[38] Mori T, Tanaka K. Acta Metall Mater 1973;21:571.
[39] Ashton JE, Halpin JC, Petit PH. Primer on composite materials: analysis. Westport, CT, USA: Technomic; 1969.
[40] Halpin JC. J Compos Mater 1969;3:732.
[41] Halpin JC, Kardos JL. Polym Eng Sci 1976;16:344.
[42] Cox HL. Br J Appl Phys 1952;3:72.
[43] Hill R. Proc Phys Soc A 1952;65:349.
[44] Tucker CL, Liang E. Compos Sci Technol 1999;59:655.
[45] Usuki A, Kawasumi M, Kojima Y, Okada A, Kurauchi T, Kamigaito O. J Mater Res 1993;8(5):1174.
[46] Segal VM, Hartwig KT, Goforth RE. Mater Sci Eng A 1997;224:107.
[47] Li CKY. Novel equal channel angular extrusion process for improving physical and mechanical properties of polymers, PhD dissertation, Texas A and M University, Department of Mechanical Engineering; 1999.
[48] Li CKY, Xia ZY, Sue HJ. Polymer 2000;41:6285.
[49] Xia ZY, Sue HJ, Hsieh AJ. J Appl Polym Sci 2001;79:2060.
[50] Xia ZY, Sue HJ, Rieker TP. Macromolecules 2000;33:8746.
[51] Weon JI, Creasy TS, Sue HJ, Hsieh A. J Polym Eng Sci 2005;45:314.
[52] Kohan MI. Nylon plastics handbook. Cincinnati, OH, USA: Hanser/Gardner; 1995.
[53] Babatope B, Isaac DH. Polymer 1992;33:1664.
[54] Fouda IM, Oraby AH. Polym Test 1999;18:235.
[55] Murthy N, Bray R, Correale S, Moore R. Polymer 1995;36:3863.
[56] Liu X, Wu Q. Polymer 2002;43:1933.
[57] Takemori M. SPE ANTEC 1978;24:216.
[58] van Es M, Xiqiao F, van Turnhout J, van der Giessen E. Specialty polymer additives: principles and applications. In: Al-Malaika S, Golovoy AW, Wilkie CA, editors.. Malden, MA, USA: Blackwell Science; 2001. Chapter 21.
[59] Hull D, Clyne TW. An introduction to composite materials. 2nd ed. New York: Cambridge University Press; 1996.
[60] Manevitch OL, Rutledge GC. J Phys Chem B 2003;108:1428.
[61] Williams LE. Fracture of mechanics of polymer. New York: Wiley; 1984.